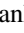
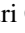



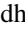




Generation of out-of-plane polarized spin current in (permalloy, Cu)/EuS interfaces

Pankhuri Gupta ¹, Niru Chowdhury ¹, Mingran Xu ^{2,3,4}, Prasanta Kumar Muduli ^{2,5}, Akash Kumar ⁶,
Kouta Kondou ³, Yoshichika Otani ^{2,3} and Pranaba Kishor Muduli ^{1,*}

¹Department of Physics, Indian Institute of Technology Delhi, Hauz Khas, New Delhi 110016, India

²Institute for Solid State Physics, University of Tokyo, Kashiwa 277-8581, Japan

³Center for Emergent Matter Science, RIKEN, 2-1 Hirosawa, Wako 351-0198, Japan

⁴École polytechnique fédérale de Lausanne (EPFL), School of Engineering, Institute of Materials, Laboratory of Nanoscale Magnetic Materials and Magnonics, 1015 Lausanne, Switzerland

⁵Department of Physics, Indian Institute of Technology Madras, Chennai 600036, India

⁶Department of Physics, University of Gothenburg, 412 96 Gothenburg, Sweden



(Received 23 October 2023; revised 31 December 2023; accepted 12 January 2024; published 12 February 2024)

The generation of out-of-plane polarized spin current is crucial for efficiently manipulating perpendicularly magnetized systems used in high-density magnetic recording. Here, we demonstrate the generation of out-of-plane polarized spin current at room temperature using an insulator, EuS. By employing angle-resolved spin-torque ferromagnetic resonance, we find a large unconventional out-of-plane torque conductivity, $\sigma_{DL}^z = -0.13 \times 10^5 (\hbar/2e) (\Omega \text{ m})^{-1}$ in the Py(= Ni₈₁Fe₁₉)/EuS bilayer, which is comparable to the conventional in-plane dampinglike torque conductivity, σ_{DL}^y . Additionally, a giant in-plane fieldlike torque (σ_{FL}^z) with a magnitude of 27 times larger than that of the conventional out-of-plane fieldlike torque (σ_{FL}^y) is also observed in the Py/EuS bilayer. The unconventional torques due to the out-of-plane polarized spin current (σ_{DL}^z and σ_{FL}^z) persist even by inserting a 10-nm-thick Cu layer between Py and EuS. Our findings demonstrate that the unconventional torques in these systems originate from the interfaces through spin swapping and/or spin-orbit precession mechanisms.

DOI: [10.1103/PhysRevB.109.L060405](https://doi.org/10.1103/PhysRevB.109.L060405)

Electrical manipulation of magnetization via spin current-induced spin-orbit torques (SOTs) has emerged as a promising method for developing advanced spintronic devices such as magnetic random access memory (MRAM) [1], spin Hall nano-oscillator (SHNO) [2–6], and magnetic nonvolatile logic devices [7], as well as emerging neuromorphic devices [8–12]. In the ferromagnetic (FM)/heavy metal (HM) structure, SOTs are generated in the bulk of HM via the spin Hall effect [13–16] and/or at the interface via the Rashba-Edelstein effect (REE) [17,18]. Both of these mechanisms lead to a so-called conventional SOT [16,19,20], in which the direction of current flow, the direction of the flow of spin current, and the direction of spin polarization of the electrons are mutually orthogonal to each other. Therefore, if the current flow is along in the x direction, the spin current generated along the z direction will have the spin polarization along the y direction. However, such conventional SOT cannot produce deterministic switching of the FM layer with the perpendicular magnetic anisotropy used in high-density magnetic recording [20–24]. Several recent studies have shown the presence of unconventional spin-orbit torques (USOTs), especially the presence of torque due to a spin polarization along the z direction (out of the film plane) by using materials with reduced crystalline symmetry (such as WTe₂ [25,26] and MoTe₂ [27]) and low magnetic symmetry (such as Mn₃GaN [28], Mn₃SnN [29], and Mn₃Sn [30]). More

recently, it has been shown that USOT can also arise from the interface between an FM and an antiferromagnet [31,32]. The USOT is essential for achieving zero-field switching of magnets with perpendicular magnetic anisotropy. However, the current shunting effect in these metallic systems leads to an overall decrease in the device efficiency. Therefore, a possible efficient approach for generating out-of-plane spin polarization for next-generation high-performance spintronic applications is using insulating materials, such as insulating antiferromagnet NiO by using interfacial effects [33]. The potential of paramagnetic insulator (PI)-based heterostructures to generate USOT, similar to the antiferromagnetic insulator-based systems, remains an open question. Recently, PI/nonmagnetic (NM) bilayer systems have garnered significant attention. Despite the absence of long-range order in PI, phenomena such as spin Hall magnetoresistance (SMR) and the spin Seebeck effect (SSE) have been observed in PI/NM systems [34–36].

However, most of the investigations of PI focused on the oxide paramagnetic insulators, which must be grown under an oxygen atmosphere at high temperatures [37,38]. Therefore, on-chip integration of these PI in nanoscale spintronic devices involving metallic electrodes is complex. To this end, we chose europium sulfide EuS, a material easily deposited without requiring a high substrate temperature. Furthermore, EuS is shown to be compatible with nanoscale spintronic devices [39]. EuS is a well-known Heisenberg ferromagnetic insulator with a Curie temperature $T_C^{\text{EuS}} = 16.5 \text{ K}$ [40]. In

*muduli@physics.iitd.ac.in

its ferromagnetic state, EuS is well known for generating a giant interfacial exchange field in superconducting Al-EuS devices [41–43]. A large interfacial exchange field at the interface of EuS with two-dimensional (2D) materials such as graphene and WSe₂ has been demonstrated in several experiments [44,45]. Recently, Gomez-Perez *et al.* estimated the interfacial exchange field at the EuS/Pt interface to be ≈ 12.4 to 16.6 T via SMR experiments [46]. While these experiments have focused on the ferromagnetic phase of EuS below T_C , the paramagnetic phase (above T_C) has not been extensively studied. Furthermore, it is worth noting that there is a lack of SOT investigations on EuS-based interfaces and heterostructures.

In this work, we demonstrate the generation of out-of-plane polarized spin current at room temperature in multilayers consisting of EuS, Py(= Ni₈₁Fe₁₉), and Cu by using spin-torque ferromagnetic resonance (STFMR). In the Py/EuS bilayer we have found a significant unconventional out-of-plane torque conductivity, $\sigma_{DL}^z = -0.13 \times 10^5 (\hbar/2e) (\Omega \text{ m})^{-1}$, due to the out-of-plane polarized spin current. The magnitude of σ_{DL}^z is comparable to the conventional in-plane dampinglike torque conductivity, σ_{DL}^y . Additionally, we have observed a giant in-plane fieldlike torque conductivity, σ_{FL}^z , in the Py/EuS system, which is nearly 27 times greater than that of the conventional out-of-plane fieldlike torque conductivity, σ_{FL}^y . An intriguing finding is that, even after introducing a 10-nanometer-thick Cu layer between Py and EuS, the unconventional torques due to the out-of-plane polarized spin current, σ_{DL}^z and σ_{FL}^z , do not disappear. The origin of the observed out-of-plane polarized spin current is explained using the spin swapping/spin-orbit precession mechanism.

Devices for STFMR measurements were fabricated in two steps using maskless photolithography. In the first step, a Ti/Au coplanar waveguide (CPW) was patterned on a Si/SiO₂ substrate via electron-beam evaporation and a subsequent lift-off process. In a second lithography step, microstrip multilayers of length (l) 150 μm and a width (w) of 20 μm were patterned on top of the prepatterned Au CPW. Microstrip multilayer Py(10 nm)/Cu(0, 10, 20 nm)/EuS (10 nm) and Py(10 nm)/Cu(10 nm) (control sample) were deposited by electron-beam evaporation in a UHV chamber (Kitano Seiki Co., Ltd.) at a base pressure of about 2×10^{-8} Torr, without breaking the vacuum between the different layers. Since the top EuS layer is highly insulating, the two-step procedure ensures good electrical contact between the bottom Py layer and the Au CPW. During deposition, the substrate stage was cooled to 5 $^\circ\text{C}$ to improve the crystalline and magnetic quality of the EuS layer [47]. Before lift-off, microstrip multilayers were capped with 5 nm AlO_x to prevent degradation. The AlO_x capping layer was deposited in a separate UHV chamber by rf sputtering at room temperature. Besides the STFMR device, a series of Py/Cu/EuS multilayers and EuS thin films were also deposited in similar conditions. The crystal structure and surface morphology of the EuS thin films were verified using x-ray diffraction (XRD) and atomic force microscopy (AFM), respectively. The magnetic property of all the thin films was characterized using a Quantum Design magnetometer.

We employ the STFMR method to measure the spin-orbit torque at room temperature [19,26]. The STFMR method

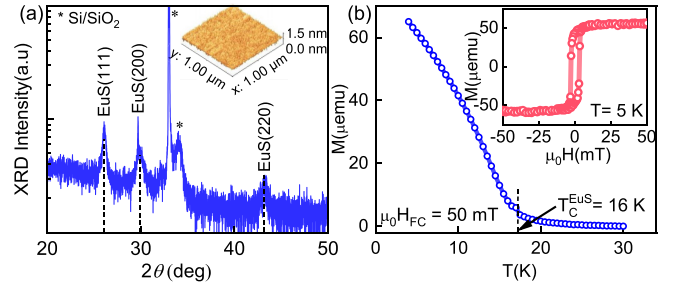


FIG. 1. (a) $\theta - 2\theta$ XRD pattern for 70 nm thick EuS film on Si/SiO₂ substrate. The peaks represent the growth of polycrystalline EuS thin film. Inset shows the AFM image of a 10 nm thick EuS film for a scan area of ($1 \times 1 \mu\text{m}^2$). (b) M-T curve for a 10 nm thick EuS film over the temperature range of 3–30 K. Inset shows in-plane hysteresis loop for the same EuS thin film at 5 K.

involves the application of a radio frequency (rf) current to the microstrip along the x direction and magnetic field applied at an angle, φ , with respect to the current direction and in the film plane (xy plane). The angle, φ , was varied from 0° to 360° with the help of a vector field magnet. The current-induced torques initiate the precession of the magnetization of the Py layer, which creates a time-dependent change in the resistance of the bilayer due to the anisotropic magnetoresistance (AMR). This change in resistance mixes with the rf current to produce a direct current voltage, V_{DC} , across the microstrip. The details of the measurement setup can be found elsewhere [31,48].

Figure 1(a) shows the XRD patterns for 70 nm thick electron-beam evaporated EuS thin films on a Si/SiO₂ substrate. XRD peaks are observed at $2\theta = 26.1^\circ$, 29.9° , and 43.2° , which we assign to (111), (200), and (220) reflections of EuS, respectively [49]. Hence our XRD data suggest the polycrystalline growth of EuS thin films. The AFM scan shown in the inset to Fig. 1(a) demonstrates that the EuS films have a smooth morphology with a root-mean-square roughness of ≈ 0.3 nm for a scan area of $1 \times 1 \mu\text{m}^2$. Figure 1(b) shows the field-cooled temperature-dependent magnetization of a 10 nm thick EuS thin film, showing a Curie temperature of 16 K. Below the Curie temperature, EuS is a soft ferromagnet with an in-plane magnetization, as demonstrated by the hysteresis loop shown in the inset of Fig. 1(b). A small field of 4 mT is sufficient to switch the in-plane magnetization and a much higher field of ≈ 1.5 T is necessary to saturate the magnetization out of plane [50]. The EuS thin films are found to be highly insulating, with resistance > 50 M Ω , which is similar to the e-beam evaporated EuS thin films reported by other groups [46]. Figure 2 shows the measured room temperature STFMR spectra obtained for the control sample Py/Cu(10), Py/EuS, Py/Cu(10)/EuS, and Py/Cu(20)/EuS, measured at 6 GHz with the in-plane magnetic field applied at an angle $\varphi = 60^\circ$ to the rf current. The measured STFMR signal (V_{DC}) is fitted by combining symmetric and antisymmetric Lorentzian functions [19]. In the following, the amplitudes of the symmetric component are denoted by V_S , while the amplitude of the antisymmetric component is denoted by V_A . The control sample Py/Cu(10) and Py/Cu(20)/EuS have predominantly antisymmetric behavior, while the Py/EuS and

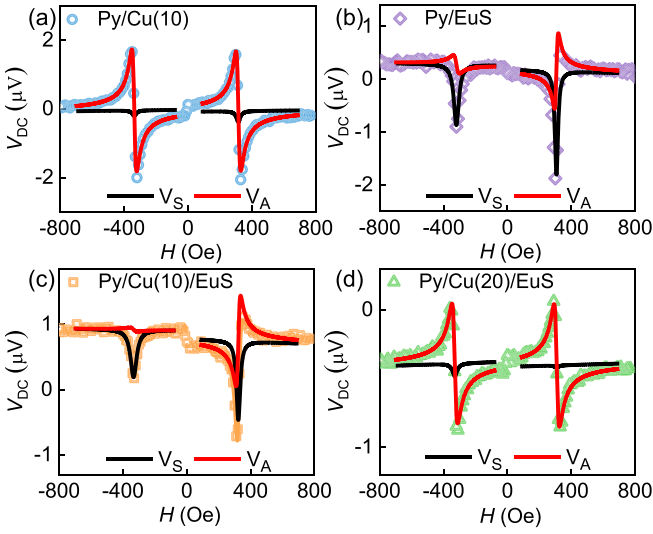


FIG. 2. Measured STFMR spectra for (a) control sample Py/Cu(10), (b) Py/EuS, (c) Py/Cu(10)/EuS, and (d) Py/Cu(20)/EuS. These spectra are measured with the magnetic field applied at an angle of $\varphi = 60^\circ$ at the rf of 6 GHz and injected rf power of -5 dBm.

Py/Cu(10)/EuS samples exhibit larger symmetric components. In the case of conventional SOT, the field polarity reversal only leads to a change in the sign of both the symmetric (V_S) and antisymmetric voltage components (V_A) of the rectified voltage, i.e., $V_{S,A}(H > 0) = -V_{S,A}(H < 0)$ [19,26]. This is found to be the case for the control sample Py/Cu and Py/Cu(20)/EuS [Figs. 2(a) and 2(d)], for which we found $V_A(H > 0) = -V_A(H < 0)$ and $V_S \ll V_A$. In contrast, for the case of Py/EuS and Py/Cu(10)/EuS [Figs. 2(b) and 2(c)], (1) both the antisymmetric and symmetric components exhibit a change of the magnitude with field polarity reversal [i.e., $|V_{S,A}(H > 0)| \neq |V_{S,A}(H < 0)|$] and (2) the symmetric component does not change sign with field polarity reversal. These results suggest the presence of an unconventional spin-orbit torque (USOT) in the case of Py/EuS and Py/Cu(10)/EuS.

We analyze the results in more detail by performing complete angular dependence of the STFMR. Figure 3 shows the angular dependence for the symmetric (black) and antisymmetric (red) STFMR signal. The angular dependence of V_S and V_A in the control sample Py/Cu(10) and Py/Cu(20)/EuS display a small symmetric component and a substantial antisymmetric component in agreement with Fig. 2. The asymmetric components in these two samples clearly follow the conventional $\sin(2\varphi)\cos(\varphi)$ dependence.

In contrast, the samples Py/EuS and Py/Cu(10)/EuS exhibit significant deviation from the conventional $\sin(2\varphi)\cos(\varphi)$ behavior [19,26]. To account for this deviation, an extra term proportional to $\sin(2\varphi)$ is introduced, corresponding to a spin polarization in the z direction. The angular dependence of V_S and V_A are fitted using [26,28,51]

$$V_S = S_{DL}^y \sin(2\varphi)\cos(\varphi) + S_{FL}^z \sin(2\varphi), \quad (1)$$

$$V_A = A_{FL}^y \sin(2\varphi)\cos(\varphi) + A_{DL}^z \sin(2\varphi). \quad (2)$$

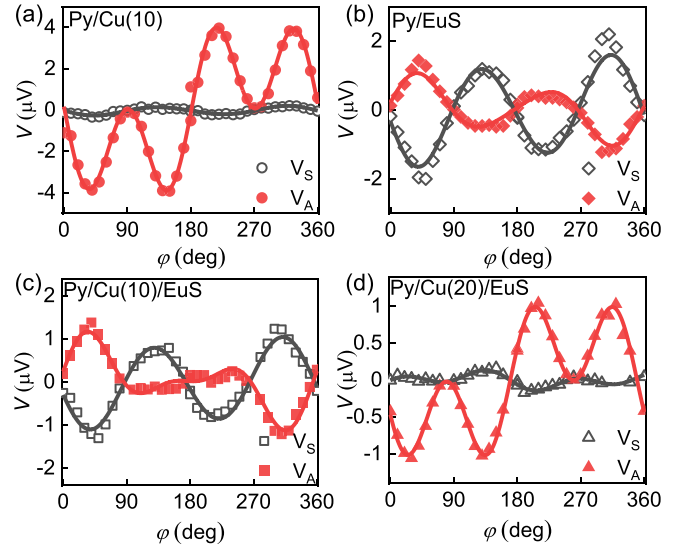


FIG. 3. Symmetric and antisymmetric STFMR components for (a) control sample Py/Cu(10), (b) Py/EuS, (c) Py/Cu(10)/EuS, and (d) Py/Cu(20)/EuS as a function of in-plane magnetic field angle (φ). The fitting (solid lines) is performed using Eqs. (1) and (2).

Here, S_{DL}^y and A_{DL}^z are proportional to the dampinglike (DL) torque generated by the different components of torque conductivity tensor, σ_{zx}^y and σ_{zx}^z , respectively. Similarly, A_{FL}^y and S_{FL}^z are proportional to the corresponding fieldlike (FL) component of the torque conductivity tensor. The superscript refers to the direction of spin polarization for a charge current applied along the x direction. These fit parameters $S_{DL}^{y(z)}$ and $A_{FL}^{y(z)}$ are related to torques $\tau_{DL(FL)}^{y(z)}$ and $\tau_{FL(DL)}^{y(z)}$ by [26,27,52,53]

$$\tau_{DL(FL)}^{y(z)} = \frac{2S_{DL(FL)}^{y(z)}\alpha\gamma(2H_R + \mu_0 M_{\text{eff}})}{\Delta R I_{\text{rf}}}, \quad (3)$$

$$\tau_{FL(DL)}^{y(z)} = \frac{2A_{FL(DL)}^{y(z)}\alpha\gamma(2H_R + \mu_0 M_{\text{eff}})}{\Delta R I_{\text{rf}} \sqrt{1 + \frac{\mu_0 M_{\text{eff}}}{H_R}}}. \quad (4)$$

Here, ΔR represents the anisotropic magnetoresistance of Py. I_{rf} is the microwave current through the device. α , $\mu_0 M_{\text{eff}}$, and γ are the Gilbert damping constant, the effective magnetization, and the gyromagnetic ratio, respectively. The values of $\mu_0 M_{\text{eff}}$, H_R , and α are calculated from frequency-dependent STFMR measurements, shown in the Supplemental Material in Figs. S1 and S2 [54]. In the above equation, the torque is normalized by angular momentum and thus has the unit of frequency. The dampinglike torque component $\tau_{DL}^y \propto \hat{m} \times (\hat{m} \times \hat{y})$, while the fieldlike torque component $\tau_{FL}^y \propto \hat{m} \times \hat{y}$. These components correspond to conventional torques due to a spin polarization along the y direction. The dampinglike torque component $\tau_{DL}^z \propto \hat{m} \times (\hat{m} \times \hat{z})$ corresponds to an unconventional out-of-plane antidampinglike torque. Finally, the fieldlike torque component $\tau_{FL}^z \propto \hat{m} \times \hat{z}$ corresponds to an unconventional in-plane fieldlike torque. Both τ_{DL}^z and τ_{FL}^z arise due to an out-of-plane spin polarization in the z direction.

To compare the strength of the observed torques in our devices, we calculate the ratio between the different components of torque: τ_{DL}^y/τ_{FL}^y , τ_{DL}^z/τ_{FL}^z , and τ_{FL}^z/τ_{DL}^z . τ_{DL}^y/τ_{FL}^y represents

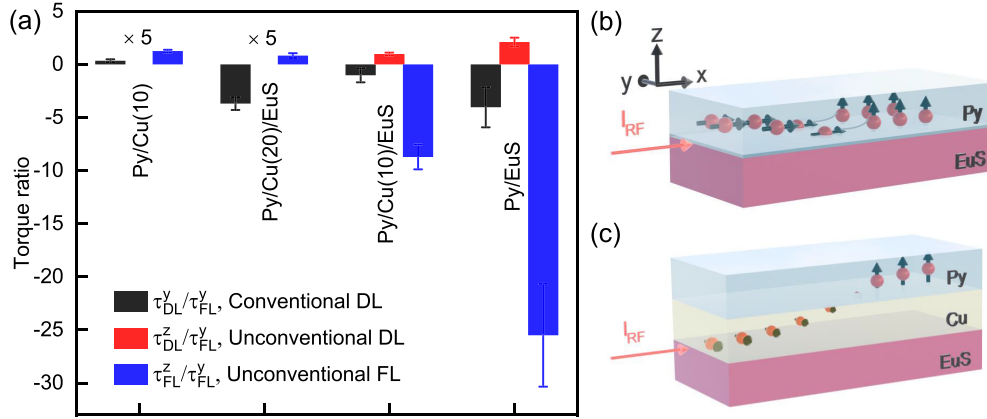


FIG. 4. (a) Torque ratios for control sample Py/Cu, Py/Cu(10)/EuS, Py/Cu(20)/EuS, and Py/EuS. The ratio τ_{DL}^y/τ_{FL}^y represents the conventional DL torque ratio (black), while τ_{DL}^z/τ_{FL}^y and τ_{FL}^z/τ_{FL}^y represent the unconventional DL torque ratio (red) and unconventional FL torque ratio (blue), respectively. The torque ratios for the control sample Py/Cu, Py/Cu(20)/EuS are multiplied by a factor of 5 to enhance the visibility of the torque ratios in the plot. (b) Schematic illustration of generation of out-of-plane spin-polarized current via the “spin-swapping” mechanism in a Py/EuS bilayer. (c) Schematic illustration of generation of an out-of-plane spin-polarized current in the Py/Cu/EuS trilayer via a combination of REE at the Cu/EuS interface and “spin-orbit precession” mechanism at the Py/Cu interface.

the torque ratio for the conventional torque. τ_{DL}^z/τ_{FL}^y and τ_{FL}^z/τ_{FL}^y represent the torque ratio for the unconventional case relative to the conventional torque τ_{FL}^y . The comparison of these three torque ratios for the four types of devices is plotted in Fig. 4(a). In Figs. 4(b) and 4(c), we also indicate inferred polarization of electrons based on our observation. In the Py/EuS sample, for which the Py layer is in direct contact with the EuS layer, we observe both conventional and unconventional torques. We observe a giant unconventional fieldlike torque with ratio $\tau_{FL}^z/\tau_{FL}^y \approx -25.5 \pm 4.8$ and a large unconventional dampinglike torque with ratio $\tau_{DL}^z/\tau_{FL}^y \approx 2.1 \pm 0.4$. Both these ratios correspond to spin polarization along the z direction. The conventional torque with spin polarization along the y direction is also significant, with ratio $\tau_{DL}^y/\tau_{FL}^y \approx -4.0 \pm 1.8$.

Since EuS is highly resistive, no current can flow in the EuS layer and hence the spin Hall effect from bulk EuS can be neglected. Thus *the torques observed are purely interfacial*. We can rule out torques from bulk Py by comparing the torque ratio with the control sample, for which all three torque ratios nearly vanish. In the case of in-plane magnetized-Py/EuS, the out-of-plane spin polarization can arise either from the spin-swapping mechanism [55] or the spin-orbit precession [56] effect at the interface. In our case, we can neglect the spin-swapping effect originating from a band structure, as the control sample exhibits negligible unconventional SOT contributions [57]. The extrinsic spin-swapping effect arises due to the spin-orbit interaction in scattering. In our case, the scattering can happen at the interface, which, in principle, can produce an out-of-plane spin polarization, as shown in Fig. 4(b). Recent results show that the spin-swapping effect can lead to a large value of τ_{FL}^z [58], which we also observe in the case of Py/EuS. The spin-orbit precession mechanism [56] can also generate an out-of-plane spin polarization due to the precession of carrier spins about the interfacial spin-orbit field while scattering off the Py/EuS interface. In the spin-orbit precession mechanism, the spin-orbit field is defined

as $\mathbf{u}(\mathbf{k}) \propto \hat{\mathbf{k}} \times \hat{\mathbf{z}}$. Here, $\hat{\mathbf{k}}$ is a unit vector pointing along the incident momentum of the electron. Hence, for electron flow along the x direction, the spin-orbit field will be along the y direction, which will produce a spin-orbit precession spin current with polarization along $\hat{m} \times \hat{y} = \hat{z}$ for the in-plane magnetization of the Py layer. Recent experimental results show that the spin-orbit precession mechanism largely produces τ_{DL}^z [59,60]. Since we also observe a large τ_{DL}^y in the case of Py/EuS, we cannot rule out the spin-orbit precession mechanism for the observed unconventional SOT. Thus we attribute the observed unconventional torques in Py/EuS to a combination of spin swapping and the spin-orbit precession mechanism. Since the extrinsic spin-swapping mechanism and spin-orbit precession mechanisms are caused by spin-dependent scattering at the interfaces, our observation of the giant fieldlike torque is consistent with that of Ou *et al.* [61], in which the authors argue that the fieldlike torque originates from spin-dependent scattering at the interface. However, in contrast to Ou *et al.* [61], we observe a giant unconventional in-plane fieldlike torque τ_{FL}^z due to the out-of-plane spin polarization, which originates from a more complex generalization spin-dependent scattering at the Py/EuS interface.

Now, we will discuss the possible origin of unconventional SOT in Py/Cu(10)/EuS. Interestingly, the unconventional torques persist even after inserting a 10-nm-thick Cu layer between Py and EuS. This result is somewhat surprising. Since the Cu layer breaks the interface between Py and EuS, one would expect the torques arising from the interface between Py and EuS to vanish entirely by inserting the Cu layer. The unconventional torque vanishes (but not entirely) only for 20-nm-thick Cu. Since Cu has a negligible bulk spin-orbit coupling, we do not expect interfacial torques from the Py/Cu interface, which is further confirmed by the control sample, for which no conventional and unconventional torques are observed. Thus our results indicate that unconventional torques in Py/Cu(10)/EuS arise from a spin accumulation at

the Cu/EuS interface via the Rashba-Edelstein effect (REE). The accumulated spin exchange couples to the magnetization of the Py layer across the Cu layer, producing a SOT. This is similar to a nonlocal Rashba-Edelstein field discussed by Emori *et al.* [62] in the Py/Cu/Al₂O₃ system. However, the mechanism proposed by S. Emori *et al.* can only produce conventional torques since the REE produces spin polarization along the y axis. Hence we believe the unconventional torques with spin polarization along the z axis are created due to the spin swapping and/or spin-orbit precession mechanism [55–60] at the Py/Cu interface, similar to the Py/EuS interface. A calculation based on a parallel resistor model shows that, in the case of Py/Cu(10)/EuS, 94% of the current flows in the Cu layer. Thus the current in the Py layer can be neglected. The current flowing through the Cu layer can get spin polarized due to the REE at the Cu/EuS interface, which consequently produces a spin current with polarization along the z axis due to spin swapping and/or the spin-orbit precession mechanism at the Py/Cu interface, as shown in Fig. 4(c). This is also consistent with the presence of both τ_{FL}^z and τ_{DL}^z in Py/Cu(10)/EuS. We also independently confirm the presence of REE in Py/Cu(10)/EuS samples by performing inverse REE measurements, as shown in Supplemental Material Sec. S3 [54]. Therefore, the simultaneous action of REE at the Cu/EuS interface and the spin swapping/spin-orbit precession mechanism at the Py/Cu interface determine the generation of out-of-plane spin polarization and unconventional torques in Py/Cu(10)/EuS. As the thickness of Cu is increased to 20 nm, the spin accumulation at Py/Cu due to REE at the Cu/EuS interface decreases, producing a significantly lower unconventional SOT.

Finally, we quantify the strength of the individual components of the torques. We define the torque conductivity as nominally independent of geometric factors. It is defined as the amount of angular momentum the magnet absorbs per second, per unit interface area, and per unit electric field. For each torque value, $\tau_{\text{DL,FL}}^{y,z}$, the torque conductivity can be defined as [26,27]

$$\sigma_{\text{DL,FL}}^{y,z} = \frac{M_S l w t_{\text{Py}} \tau_{\text{DL,FL}}^{y,z}}{\gamma (lw) E} = \frac{M_S l t_{\text{Py}} \tau_{\text{DL,FL}}^{y,z}}{\gamma I_{\text{rf}} Z}. \quad (5)$$

Here M_S is the saturation magnetization which is approximated as M_{eff} , E is the electric field, l and w are the length and width of the microstrip, t_{Py} is the thickness of the Py layer, and Z is the device impedance. I_{rf} is the microwave current through the device, which we calculated by measuring S_{11} using a vector network analyzer, as discussed in Supplemental Material Sec. S2 [54] (see also Ref. [63] therein). Using Eq. (5), we found spin torque conductivity [in units of $10^5 \hbar/2e$ (Ωm)⁻¹] as $\sigma_{\text{DL}}^z = (-0.13 \pm 0.01)$ and $\sigma_{\text{FL}}^z = (1.61 \pm 0.07)$, $\sigma_{\text{DL}}^y = (0.25 \pm 0.11)$, and $\sigma_{\text{FL}}^y =$

(-0.06 ± 0.01) for the Py/EuS sample. Thus the in-plane fieldlike torque (σ_{FL}^z) has a magnitude which is nearly 27 times larger than that of the conventional out-of-plane fieldlike torque (σ_{FL}^y) in Py/EuS. For Py/Cu(10)/EuS we found $\sigma_{\text{DL}}^z = (-0.13 \pm 0.01)$, $\sigma_{\text{FL}}^z = (1.20 \pm 0.09)$, $\sigma_{\text{DL}}^y = (0.14 \pm 0.09)$, and $\sigma_{\text{FL}}^y = (-0.14 \pm 0.01)$. The value of both conventional and unconventional torque conductivities (σ_{DL}^y and σ_{FL}^z) are found to be larger compared to the corresponding torques measured in low-symmetry transition metal dichalcogenides (TMDs) based systems such as WTe₂/Py [26], MoTe₂/Py [27], and NbSe₂/Py [64]. It should be noted that the values we obtained cannot be compared to those reported in Mn₃GaN [28], Mn₃SnN [29], and Mn₃Sn [30], since the origin of USOT in these reports is not interfacial.

In conclusion, we have observed the generation of out-of-plane polarized spin currents at room temperature utilizing insulating EuS. A large out-of-plane dampinglike and a giant in-plane fieldlike torque is observed in Py/EuS due to out-of-plane polarized spin currents. The origin of the observed USOT is purely interfacial and we explain it using a hybrid spin swapping/spin-orbit precession mechanism. The presence of unconventional torques for devices with a 10-nanometer-thick Cu layer between Py and EuS is explained using the simultaneous action of REE at the Cu/EuS interface and the spin swapping/spin-orbit precession mechanism at the Py/Cu interface. Our findings of the generation of out-of-plane polarized spin currents at room temperature, using nonoxide insulating paramagnetic EuS, have high technological relevance for energy-efficient CMOS-compatible spintronic devices.

The partial support from the Ministry of Human Resource Development under the IMPRINT program (Grants No. 7519 and No. 7058), the Department of Electronics and Information Technology (DeitY), Science and Engineering research board (SERB File No. CRG/2018/001012 and No. CRG/2022/002821), Joint Advanced Technology Centre at IIT Delhi, Grand Challenge Project, IIT Delhi, and the Department of Science and Technology under the Nanomission program [Grant No. SR/NM/NT-1041/2016(G)] are gratefully acknowledged. P.G. acknowledges support from the Ministry of Human Resource Development (MHRD), India. N.C. acknowledges support from the Chanakya Post Doctoral Fellowship. P.K.M. acknowledges funding from IIT Madras (Grants No. IP21221798PHNFSC008989 and No. RF21221392PHNFIG008989) and Science and Engineering Research Board (SERB), India, Grant No. SRG/2022/000438. M.X. would like to thank support from JSPS through “Research program for Young Scientists” (no. 19 J21720) and RIKEN IPA Program. Finally, we also thank N. Leo for insightful comments on the manuscript.

- [1] Z. He, Y. Zhang, S. Angizi, B. Gong, and D. Fan, *IEEE Trans. Multi-Scale Comput. Syst.* **4**, 676 (2018).
 [2] V. E. Demidov, S. Urazhdin, H. Ulrichs, V. Tiberkevich, A. Slavin, D. Baither, G. Schmitz, and S. O. Demokritov, *Nat. Mater.* **11**, 1028 (2012).

- [3] A. A. Awad, P. Dürrenfeld, A. Houshang, M. Dvornik, E. Iacocca, R. K. Dumas, and J. Åkerman, *Nat. Phys.* **13**, 292 (2017).
 [4] T. Chen, R. K. Dumas, A. Eklund, P. K. Muduli, A. Houshang, A. A. Awad, P. Dürrenfeld, B. G. Malm, A. Rusu, and J. Åkerman, *Proc. IEEE* **104**, 1919 (2016).

- [5] N. Behera, H. Fulara, L. Bainsla, A. Kumar, M. Zahedinejad, A. Houshang, and J. Åkerman, *Phys. Rev. Appl.* **18**, 024017 (2022).
- [6] A. Kumar, H. Fulara, R. Khymyn, A. Litvinenko, M. Zahedinejad, M. Rajabali, X. Zhao, N. Behera, A. Houshang, A. A. Awad, and J. Åkerman, *Nano Lett.* **23**, 6720 (2023).
- [7] A. Kurenkov, S. D. Gupta, C. Zhang, S. Fukami, Y. Horio, and H. Ohno, *Adv. Mater.* **31**, 1900636 (2019).
- [8] M. Zahedinejad, A. A. Awad, S. Muralidhar, R. Khymyn, H. Fulara, H. Mazraati, M. Dvornik, and J. Åkerman, *Nat. Nanotechnol.* **15**, 47 (2020).
- [9] A. Houshang, M. Zahedinejad, S. Muralidhar, J. Chечиński, R. Khymyn, M. Rajabali, H. Fulara, A. A. Awad, M. Dvornik, and J. Åkerman, *Phys. Rev. Appl.* **17**, 014003 (2022).
- [10] N. Garg, S. V. H. Bhotla, P. K. Muduli, and D. Bhowmik, *Neuromorph. Comput. Eng.* **1**, 024005 (2021).
- [11] A. Kumar, M. Rajabali, V. H. González, M. Zahedinejad, A. Houshang, and J. Åkerman, *Nanoscale* **14**, 1432 (2022).
- [12] R. S. Yadav, P. Gupta, A. Holla, K. I. Ali Khan, P. K. Muduli, and D. Bhowmik, *ACS Appl. Electron. Mater.* **5**, 484 (2023).
- [13] M. I. Dyakonov and V. I. Perel, *Phys. Lett. A* **35**, 459 (1971).
- [14] J. E. Hirsch, *Phys. Rev. Lett.* **83**, 1834 (1999).
- [15] J. Sinova, S. O. Valenzuela, J. Wunderlich, C. H. Back, and T. Jungwirth, *Rev. Mod. Phys.* **87**, 1213 (2015).
- [16] A. Manchon, J. Železný, I. M. Miron, T. Jungwirth, J. Sinova, A. Thiaville, K. Garello, and P. Gambardella, *Rev. Mod. Phys.* **91**, 035004 (2019).
- [17] Y. A. Bychkov and É. I. Rashba, *Pis'ma Zh. Eksp. Teor. Fiz.* **39**, 66 (1983) [*JETP Lett.* **39**, 78 (1984)].
- [18] V. M. Edelstein, *Solid State Commun.* **73**, 233 (1990).
- [19] L. Liu, T. Moriyama, D. C. Ralph, and R. A. Buhrman, *Phys. Rev. Lett.* **106**, 036601 (2011).
- [20] L. Liu, C. F. Pai, Y. Li, H. Tseng, D. Ralph, and R. Buhrman, *Science* **336**, 555 (2012).
- [21] I. M. Miron, K. Garello, G. Gaudin, P. J. Zermatten, M. V. Costache, S. Auffret, S. Bandiera, B. Rodmacq, A. Schuhl, and P. Gambardella, *Nature (London)* **476**, 189 (2011).
- [22] G. Yu, P. Upadhyaya, Y. Fan, J. G. Alzate, W. Jiang, K. L. Wong, S. Takei, S. A. Bender, L.-T. Chang, Y. Jiang *et al.*, *Nat. Nanotechnol.* **9**, 548 (2014).
- [23] L. Liu, O. J. Lee, T. J. Gudmundsen, D. C. Ralph, and R. A. Buhrman, *Phys. Rev. Lett.* **109**, 096602 (2012).
- [24] S. Fukami, T. Anekawa, C. Zhang, and H. Ohno, *Nat. Nanotechnol.* **11**, 621 (2016).
- [25] D. MacNeill, G. M. Stiehl, M. H. D. Guimaraes, N. D. Reynolds, R. A. Buhrman, and D. C. Ralph, *Phys. Rev. B* **96**, 054450 (2017).
- [26] D. MacNeill, G. M. Stiehl, M. H. D. Guimaraes, R. A. Buhrman, J. Park, and D. C. Ralph, *Nat. Phys.* **13**, 300 (2017).
- [27] G. M. Stiehl, R. Li, V. Gupta, I. El Baggari, S. Jiang, H. Xie, L. F. Kourkoutis, K. F. Mak, J. Shan, R. A. Buhrman, and D. C. Ralph, *Phys. Rev. B* **100**, 184402 (2019).
- [28] T. Nan, C. X. Quintela, J. Irwin, G. Gurung, D. F. Shao, J. Gibbons, N. Campbell, K. Song, S. Y. Choi, L. Guo, R. D. Johnson, P. Manuel, R. V. Chopdekar, I. Hallsteinsen, T. Tybell, P. J. Ryan, J. W. Kim, Y. Choi, P. G. Radaelli, D. C. Ralph *et al.*, *Nat. Commun.* **11**, 4671 (2020).
- [29] Y. You, H. Bai, X. Feng, X. Fan, L. Han, X. Zhou, Y. Zhou, R. Zhang, T. Chen, F. Pan, and C. Song, *Nat. Commun.* **12**, 6524 (2021).
- [30] K. Kondou, H. Chen, T. Tomita, M. Ikhlās, T. Higo, A. H. MacDonald, S. Nakatsuji, and Y. Otani, *Nat. Commun.* **12**, 6491 (2021).
- [31] A. Kumar, P. Gupta, N. Chowdhury, K. I. A. Khan, U. Shashank, S. Gupta, Y. Fukuma, S. Chaudhary, and P. K. Muduli, *Adv. Quantum Technol.* **6**, 2300092 (2023).
- [32] S. Liang, L. Han, Y. You, H. Bai, F. Pan, and C. Song, *Phys. Rev. B* **107**, 184427 (2023).
- [33] M. Wang, J. Zhou, X. Xu, T. Zhang, Z. Zhu, Z. Guo, Y. Deng, M. Yang, K. Meng, B. He, J. Li, G. Yu, T. Zhu, A. Li, X. Han, and Y. Jiang, *Nat. Commun.* **14**, 2871 (2023).
- [34] A. Aqeel, N. Vlietstra, J. A. Heuver, G. E. W. Bauer, B. Noheda, B. J. van Wees, and T. T. M. Palstra, *Phys. Rev. B* **92**, 224410 (2015).
- [35] K. Oyanagi, S. Takahashi, T. Kikkawa, and E. Saitoh, *Phys. Rev. B* **107**, 014423 (2023).
- [36] S. M. Wu, J. E. Pearson, and A. Bhattacharya, *Phys. Rev. Lett.* **114**, 186602 (2015).
- [37] R. Luo, X. Zhao, L. Chen, T. J. Legvold, H. Navarro, I. K. Schuller, and D. Natelson, *Appl. Phys. Lett.* **121**, 102404 (2022).
- [38] D. Hirobe, M. Sato, T. Kawamata, Y. Shiomi, K. I. Uchida, R. Iguchi, Y. Koike, S. Maekawa, and E. Saitoh, *Nat. Phys.* **13**, 30 (2017).
- [39] P. K. Muduli, M. Kimata, Y. Omori, T. Wakamura, S. P. Dash, and Y. C. Otani, *Phys. Rev. B* **98**, 024416 (2018).
- [40] J. S. Moodera, T. S. Santos, and T. Nagahama, *J. Phys.: Condens. Matter* **19**, 165202 (2007).
- [41] J. S. Moodera, X. Hao, G. A. Gibson, and R. Meservey, *Phys. Rev. Lett.* **61**, 637 (1988).
- [42] X. Hao, J. S. Moodera, and R. Meservey, *Phys. Rev. Lett.* **67**, 1342 (1991).
- [43] E. Strambini, V. N. Golovach, G. De Simoni, J. S. Moodera, F. S. Bergeret, and F. Giazotto, *Phys. Rev. Mater.* **1**, 054402 (2017).
- [44] P. Wei, S. Lee, F. Lemaître, L. Pinel, D. Cutaia, W. Cha, F. Katmis, Y. Zhu, D. Heiman, J. Hone, J. S. Moodera, and C.-T. Chen, *Nat. Mater.* **15**, 711 (2016).
- [45] C. Zhao, T. Norden, P. Zhang, P. Zhao, Y. Cheng, F. Sun, J. P. Parry, P. Taheri, J. Wang, Y. Yang, T. Scrace, K. Kang, S. Yang, G. Miao, R. Sabirianov, G. Kioseoglou, W. Huang, A. Petrou, and H. Zeng, *Nat. Nanotechnol.* **12**, 757 (2017).
- [46] J. M. Gomez-Perez, X. P. Zhang, F. Calavalle, M. Ilyn, C. González-Orellana, M. Gobbi, C. Rogero, A. Chuvilin, V. N. Golovach, L. E. Hueso, F. S. Bergeret, and F. Casanova, *Nano Lett.* **20**, 6815 (2020).
- [47] G. X. Miao and J. S. Moodera, *Appl. Phys. Lett.* **94**, 182504 (2009).
- [48] A. Kumar, R. Sharma, K. I. Ali Khan, C. Murapaka, G. J. Lim, W. S. Lew, S. Chaudhary, and P. K. Muduli, *ACS Appl. Electron. Mater.* **3**, 3139 (2021).
- [49] A. Tanaka, H. Kamikubo, Y. Doi, Y. Hinatsu, M. Kataoka, T. Kawai, and Y. Hasegawa, *Chem. Mater.* **22**, 1776 (2010).
- [50] P. Muduli, N. Leo, M. Xu, Z. Zhu, J. Puebla, C. Ortiz, H. Isshiki, and Y. Otani, Non-equilibrium spin polarisation via interfacial exchange-field spin filtering, [arXiv:2308.13855](https://arxiv.org/abs/2308.13855).
- [51] A. Bose, N. J. Schreiber, R. Jain, D. F. Shao, H. P. Nair, J. Sun, X. S. Zhang, D. A. Muller, E. Y. Tsymbal, D. G. Schlom, and D. C. Ralph, *Nat. Electron.* **5**, 267 (2022).

- [52] Y. Liu, Y. Liu, M. Chen, S. Srivastava, P. He, K. L. Teo, T. Phung, S. H. Yang, and H. Yang, *Phys. Rev. Appl.* **12**, 064046 (2019).
- [53] A. Mellnik, J. Lee, A. Richardella, J. Grab, P. Mintun, M. H. Fischer, A. Vaezi, A. Manchon, E. A. Kim, N. Samarth, and D. C. Ralph, *Nature (London)* **511**, 449 (2014).
- [54] See Supplemental Material at <http://link.aps.org/supplemental/10.1103/PhysRevB.109.L060405> for frequency-dependent STFM data, calibration of microwave current, and inverse Rashba Edelstein effect (IREE) measurements. The Supplemental Material also contains Ref. [63].
- [55] M. B. Lifshits and M. I. Dyakonov, *Phys. Rev. Lett.* **103**, 186601 (2009).
- [56] V. P. Amin, J. Zemen, and M. D. Stiles, *Phys. Rev. Lett.* **121**, 136805 (2018).
- [57] H. J. Park, H. W. Ko, G. Go, J. H. Oh, K. W. Kim, and K. J. Lee, *Phys. Rev. Lett.* **129**, 037202 (2022).
- [58] B. K. Hazra, B. Pal, J. C. Jeon, R. R. Neumann, B. Göbel, B. Grover, H. Deniz, A. Styervoyedov, H. Meyerheim, I. Mertig, S. H. Yang, and S. S. P. Parkin, *Nat. Commun.* **14**, 4549 (2023).
- [59] C. B. Seung Heon, V. P. Amin, Y. W. Oh, G. Go, S. J. Lee, G. H. Lee, K. J. Kim, M. D. Stiles, B. G. Park, and K. J. Lee, *Nat. Mater.* **17**, 509 (2018).
- [60] Y. Hibino, T. Moriyama, K. Hasegawa, T. Koyama, T. Ono, and D. Chiba, *Appl. Phys. Express* **13**, 083001 (2020).
- [61] Y. Ou, C.-F. Pai, S. Shi, D. C. Ralph, and R. A. Buhrman, *Phys. Rev. B* **94**, 140414(R) (2016).
- [62] S. Emori, T. Nan, A. M. Belkessam, X. Wang, A. D. Matyushov, C. J. Babroski, Y. Gao, H. Lin, and N. X. Sun, *Phys. Rev. B* **93**, 180402(R) (2016).
- [63] K. U. Demasius, T. Phung, W. Zhang, B. P. Hughes, S. H. Yang, A. Kellock, W. Han, A. Pushp, and S. S. P. Parkin, *Nat. Commun.* **7**, 10644 (2016).
- [64] M. H. Guimaraes, G. M. Stiehl, D. MacNeill, N. D. Reynolds, and D. C. Ralph, *Nano Lett.* **18**, 1311 (2018).